Research Article | Vol. 30, No. 2 / 17 Jan 2022 / Optics Express 780
Optics EXPRESS

Optical emitter based on micro-scaled photonic structures

KWONG-KIT CHOI* AND ACHYUT K. DUTTA

Banpil Photonics, Santa Clara, CA 95054, USA
*kchoi@banpil.com

Abstract: A midwave infrared light emitting device (LED) with a micro-scaled photonic structure coupling to a resonator is proposed. The photonic structure is used to create localized surface plasmons (LSP), with which significant optical confinement can occur near the surface, thereby increasing the internal emission quantum efficiency. The LED volume is further designed into a resonator, with which the LSP resonates with the radiating mode of the resonator, thereby increasing the light extraction efficiency. The similarly designed structure can also be used as a wavelength-selective passive emitter to suppress the thermal radiation beyond a cutoff wavelength. Therefore, the designed emitter structure can be useful in a wide range of applications.

1. Introduction

The external quantum efficiency (EQE) of a light emitting device (LED) such as a light emitting diode or an interband cascade device depends on a number of factors. They are the current injection efficiency (IE), the internal emission quantum efficiency (IQE), and the light extraction efficiency (LEE). IE is mainly an electrical property of the emitter. It arises from the fact that the electrical current in a LED contains several components, which are the bulk electron and hole diffusion currents, the bulk defect assisted recombination current, and the surface leakage current. Only part of the diffusion currents participates in the carrier recombination process. IE is the portion of the total current that participates in the carrier recombination in the active layer. However, not all the carrier recombination results in light emission. Some of the carriers recombine through Auger and defect assisted processes and they are nonradiative. IQE is the fraction of radiative recombination among all the recombination processes, and it is mainly an optical property of the emitter. IQE varies widely from less than 1% to more than 80% [1], depending on the applied voltage, material band structure, and emission wavelength. LEE, on the other hand, is mainly a geometrical property of the emitter. For a simple planar structure, LEE is determined by the escape cone angle of light from the material to the air. Its value is relatively fixed at 2% for the typical semiconductor materials [2]. The small IQE, particularly in the indirect-gap and mid-infrared materials, and the small LEE in the planar geometry lead to a very small EQE in typical LEDs.

There are many ways in raising IQE and LEE of LEDs. For example, the radiative recombination rate can be increased by increasing the optical electric field in the active medium because of the increased $\mathbf{A}\cdot\mathbf{p}$ dipole transition matrix element, where $\mathbf{A}$ is vector potential operator and $\mathbf{p}$ is the momentum operator. To increase the optical electric field, a common approach is to use surface plasmon polaritons (SPPs) or localized surface plasmons (LSPs) created by metal structures [3–10]. For example, Okamoto et al. [6] utilized the large field of the SPPs generated along the interface between a planar metal layer and an InGaN LED layer and observed 6.8 times larger IQE. Fujiki et al. [7] used LSPs in metal nanoparticles (NPs) to increase the field and achieved 20-fold increase in the molecular fluorescence in organic light emitting diodes. LSP has an advantage over SPP because the resonant wavelength of LSP can be tuned to the material emission wavelength by changing their size, geometry, and spacing. Bakker et al. [10] further

#443333 https://doi.org/10.1364/OE.443333
Journal © 2022 Received 14 Sep 2021; revised 17 Nov 2021; accepted 17 Nov 2021; published 3 Jan 2022

Optics EXPRESS

utilized NPs to increase the IQE of a dye and also its LEE by designing the NPs into transmitting nanoantennae. The fluorescence enhancement in this structure can reach 100 times.

In the plasmonic structures, there is coherent cycling of energy between the light emitting medium and the plasmonic mode such that the light emission rate of the medium into the plasmonic mode is increased, similar to a cavity quantum electrodynamic (QED) system [11]. In this system, the decay rate of an excited atom is enhanced in the presence of the cavity by the Purcell factor in the weak coupling regime. In this analogy, the conduction and valence bands of the emitting medium correspond to the two atomic levels, and the plasmonic mode corresponds to the optical cavity mode. In addition to the increased emission rate, the graininess of the metal film and the geometry of the NPs transduce the evanescent, localized plasmon energy into free propagating optical energy, thereby increasing the external quantum efficiency.

Although SPP and LSP are able to improve LED's EQE, the improvement is limited by the energy loss in metal [12]. In surface plasmons, part of the optical energy is stored in electromagnetic (EM) wave in the LED medium and part of it is stored as the kinetic energy of the moving electrons in the plasma oscillations in metal. Since electrons are subjected to scattering, they lose their kinetic energy to ohmic heating. Therefore, the optical energy emitted by the LED is substantially dissipated as heat in metal, resulting in small IQE enhancement. Furthermore, there is no efficient mechanism to extract the localized surface plasmon energy into free space. The absolute LEE remains low.

On the other hand, Pendry et al. [13] showed that electromagnetic (EM) modes similar to surface plasmons can exist on a highly conducting, structured surface. This surface can even be a perfect electric conductor that does not possess electron kinetic energy and therefore does not subject to ohmic loss. The effective plasma frequency $\omega_p = (\pi/a)(c/n)$ is determined by the feature size a of the geometry, which is the linear dimension of the square holes in an array, rather than the metal material, where n is the refractive index of the dielectric surrounding the metal. The accompanied large localized field can be engineered in any spectral regions by changing its geometry. Since there is little ohmic loss in a highly conducting surface, IQE can be substantially increased. For metals such as gold and silver in the infrared and longer wavelength regimes, their electrical conductance is high, and the SPP field penetrating depth is short because of their large and negative dielectric constants [3]. As a result, these metals can serve as the highly conducting materials in these wavelength regimes. For other spectral regions, suitable materials can be identified such as NiSi in the very long infrared wavelengths [4], silver metal for the visible spectrum, and aluminum metal for the UV.

For LEE improvement, we have demonstrated a detector structure known as the resonator-pixel (RP) [14–17] whose structure is able to capture normal incident light and prevent it from leaving the active region, resulting in large infrared absorption. According to antenna reciprocity theorem, the receiving and transmitting properties of an antenna are identical, and an antenna has the same directivity in receiving and transmitting radiation power. Therefore, by treating the resonator-pixel as an antenna, its unique light capturing ability under normal incident condition will give the structure the same light transmitting ability in radiating the internal optical energy normally out to the air, resulting in a high LEE. In this work, we perform EM modeling and design optimization to show that a resonator-pixel emitter under surface plasmon resonant condition can have both large IQE and LEE to achieve a large EQE.

2. Resonator-pixel design

"Resonator-pixel" is named to distinguish its 3-dimensional geometry from the conventional 1-dimensional Fabry-Perot resonant etalon, which is also widely used to increase the LED's EQE [18–24]. In the RP detector design, the active volume is designed into a resonator to capture and store light. The detector has a top structured metal surface to diffract the normal incident light into different directions so that the light can be trapped by total internal reflection at the

Optics EXPRESS

detector boundaries. Under resonance, the trapped light interferes constructively and the internal optical intensity is increased, resulting in large absorption. For a given diffraction geometry at the surface, the diffraction angle θ_d depends on the incident wavelength λ. Whenever the internal wavelength λ_{int} is p/m, where p is periodicity of the structure and m is the diffraction order, θ_d will be close to 90°, resulting in parallel propagating light. Surface plasmon is thus created at these wavelengths. Therefore, the RP geometry creates and strengthens surface plasmons in some of its resonant eigenmodes.

In applying the RP geometry to optical emitters, the absorbing region is replaced by a light emitting region. To promote surface plasmons, the feature size a of the diffraction element, which is half of the periodicity, is designed to be close to half of the internal emission wavelength λ_{int} of the material. With this structured surface design, the emitted optical energy $\hbar\omega = \hbar 2\pi c/(n\lambda_{int}) = \hbar\pi c/(na) = \hbar\omega_p$ will be in resonance with the surface plasmon and the optical energy can be directly transferred into the plasma energy and vice versa. Similar to the natural SPP and LSP materials, the optical emission will be enhanced by these "spoof" SPP or LSP fields but the LED will not suffer from the large ohmic loss as in the visible regime. Furthermore, the volume of the resonator is designed to resonate and strengthen the surface plasmon as part of its resonant mode, with which the Purcell factor can be further increased. Since this resonant mode is also a radiating mode of the resonator, the resonator then acts as a transmitting antenna in radiating the localized energy into free space. With the RP structure, IQE and LEE can both be large, resulting in a large EQE.

Resonator-pixel geometry not only improves active emitters but also passive emitters. According to Kirchhoff's law under thermodynamic equilibrium, the emissivity of an object is equal to its absorptivity, which is another name for the external absorption quantum efficiency. Therefore, the large absorptivity of an RP under resonance will also give the structure the same large emissivity at that wavelength. This feature can be utilized to produce a spectrally selective thermal emitter at an elevated temperature. This emitter structure will be simpler to make than that using 3-dimensional photonic crystals on the material emitting surface [25].

Other than increasing the optical throughput and efficiency, the RP emitter uses a very thin active material to reduce reabsorption of light and does not require additional anti-reflection coating or distributed Bragg reflectors [18–23]. It emits from the surface rather than from the edge, and the structured metal surface enables effective thermal management. Therefore, the RP geometry has many advantages in optical emission other than offering a large EQE.

In the present design, the structured metal surface is in the form of periodic square rings with rounded corners. With a square ring design rather than a grating design, localized surface plasmons can be created within each ring similar to that of a nanoparticle. The generated electric field is then solely a property of the unit cell. The emitter characteristics will not change with the number of unit cells in a large area emitter. With this more complicated periodic structure, the predicted ω_p based on periodic hole arrays is not strictly applicable. The designed dimensions require 3-dimensional electromagnetic (EM) modeling.

A RP emitter containing 3×3 unit cells is shown in Fig. 1. In this structure, the light emitting layer is sandwiched between a top contact layer and a ground contact layer. The top contact layer is etched into a periodic ring array. A metal layer is then deposited onto the rings to form the structured surface. At the top contact/light emitting layer interface and the ground contact/substrate interface, optically thin etch-stop layers are inserted to facilitate device processing in the ring formation and substrate removal. The contact layers are wider bandgap materials with opposite doping. The top contact is usually p-doped ($\sim 2 \times 10^{18}$ cm^{-3}) and the bottom contact is usually n-doped ($\sim 1 \times 10^{18}$ cm^{-3}). The light emitting layer may consist of either a single quantum well or a multiple quantum well structure (MQW), and it is undoped [18–23]. The metal contacts are Ti/Au for p-type contact and Ge/Au for n-type contact. Alternatively, the LED can also be made of interband cascade (IC) materials [24]. Since the top

Optics EXPRESS

contact layer is partially removed from etching in forming the ring structure, Schottky contact instead of ohmic contact is formed outside the ring region. The current injection to the light emitting layer is therefore primarily through the p-type top ring contacts. The pixel sidewalls are encapsulated with a low refractive index material such as epoxy glue. Electrical contacts to the external power supply are made at the top gold layer and the ground contact layer surrounding the emitter array. Light exits through the ground contact layer into the air as shown in Fig. 1.

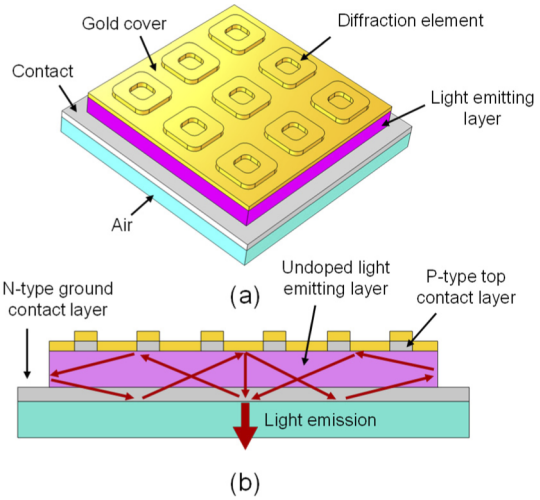

Fig. 1. (a) The 3D perspective of a resonator-pixel. Light exits from the bottom. (b) The cross-section and one possible optical path in light emission.

3. Resonator-pixel EM modeling

According to the antenna reciprocity theorem, a good transmitting antenna is also a good receiving antenna. One can first design a good detector structure and replace the absorbing material with an emitting material to achieve a good emitter. To perform optical design of a RP detector, we employ finite-element method (FEM). FEM solves the electromagnetic wave equation,

$$\nabla \times (\mu_r^{-1} \nabla \times \boldsymbol{E}) - k_0^2 \varepsilon_{rc} \boldsymbol{E} = 0, \tag{1}$$

via trial functions under a user defined boundary condition. In Eq. (1), μ_r and $\varepsilon_{rc} = \varepsilon_r - j\varepsilon_i$ are the relative permeability and relative permittivity, respectively, $k_0 = 2\pi/\lambda$ is the wavevector, and λ is the wavelength in free space. Through variational principles, FEM transforms Eq. (1) into a large set of linear equations, which can be solved by matrix multiplications. FEM provides highly accurate solution to any optical geometry with well-defined physical geometry and material optical properties. In the FEM analysis, the external absorption quantum efficiency η is given by [15]

$$\eta = \frac{1}{A} \frac{n\alpha}{E_0^2} \int_V |E|^2 d^3 r \,, \tag{2}$$

where A is the detector area, n is the refractive index of the absorbing material, E_0 is the incident electric field from air, V is the active volume, and |E| is the modeled E magnitude. The absorption coefficient α is $4\pi k/\lambda$, where k is the extinction coefficient of the absorbing material. Using Eq. (2) to know QE, the detector geometry is varied until it gives a maximum value of η. The resulting detector geometry will also be the optimal geometry for the emitter.

In this work, the goal is to design a RP emitter emitting at $\lambda \approx 4.1$ μm using AlInAs/InAsSb MQWs [23] or GaSb based IC materials [24]. Assuming n = 3.735 for this material, the internal

Optics EXPRESS

emission wavelength $\lambda_{int} = \lambda/n = 1.1$ μm. The initial setting of the inner dimension of the ring is then equal to $\lambda_{int}/2 \approx 0.5$ μm and the outer dimension of the ring is $3\lambda_{int}/2 \approx 1.5$ μm as in a regular grating. The ring height is $\lambda_{int}/4 = 0.27$ μm to eliminate zeroth order diffraction (i.e. back reflection), and the ring period is $2\lambda_{int} \approx 2$ μm. With this small ring period, a typical emitter will contain many unit cells, with which periodic boundary condition can be applied to a single unit cell to obtain the valid EM solution. The unit cell geometry, shown in Fig. 2, is then used for design optimization. If a small area emitter is employed such as the one containing 3×3 rings in Fig. 1, the entire structure can be modeled instead.

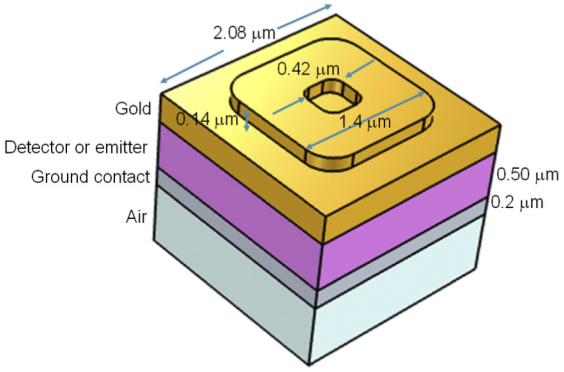

Fig. 2. The 3D perspective view of an optimized RP unit cell with $d_s = 0.42$ μm, $d_o = 1.4$ μm, $h_r = 0.14$ μm, $p = 2.08$ μm, $t_m = 0.3$ μm, $t_d = 0.5$ μm, and $t_g = 0.2$ μm. The detector $n = 3.735$, and the contact $n = 3.5$.

Based on Eq. (2), the value of η is computed with a set of adjustable detector parameters including the inner ring dimension d_s, outer ring dimension d_o, ring height h_r, unit cell dimension p, metal thickness t_m, detector active thickness t_d, and ground contact thickness t_g. In computer programming, the value of η is evaluated for different sets of structural parameters until η at $\lambda = 4.1$ μm is maximized. In this modeling, a wavelength-independent absorption coefficient α of 2000 cm^{-1} is assumed so that η is unaffected by the material absorption properties. The refractive index of gold is shown in Fig. 3. Since the Ti layer in the Ti/Au contact is atomically thin, it is not included in the EM modeling.

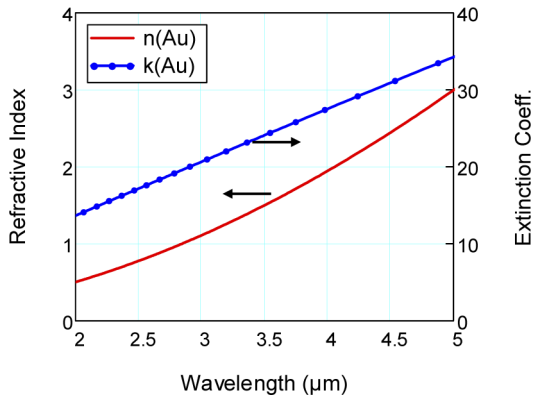

Fig. 3. The refractive index of gold adopted in the EM modeling.

After computer optimization, the optimized detector parameters are listed in Fig. 2, and the η spectrum is shown in Fig. 4. The RP detector has a QE of 76.3% at 4.08 μm compared to the

Optics EXPRESS

$\eta_{pl} = 12.5\%$ for a planar detector having two passes of light based on a ray-tracing formula given by

$$\eta_{pl} = \frac{4n}{(1+n)^2}(1 - e^{-2t_d\alpha}) \, . \tag{3}$$

This large RP QE is enabled by the strong plasmonic E field near the gold ring. It is evident in the largest gold absorption of 23.7% at this wavelength due to the enhanced plasmon oscillations in the gold layer. The other resonant peaks at the shorter wavelengths also achieved large η but they are not necessarily caused by plasmonic excitations as indicated by the E field distributions in different wavelength regimes shown in Ref. 16. For example, in the shorter λ regime, the field is more uniformly distributed within the volume where collective optical diffraction among the rings dominates. In the mid λ regime, the field is more localized within the unit cell as individual rings act as Fresnel lenses. In the long λ regime, the E field is evanescent away from the metal surface when the rings become plasmonic couplers.

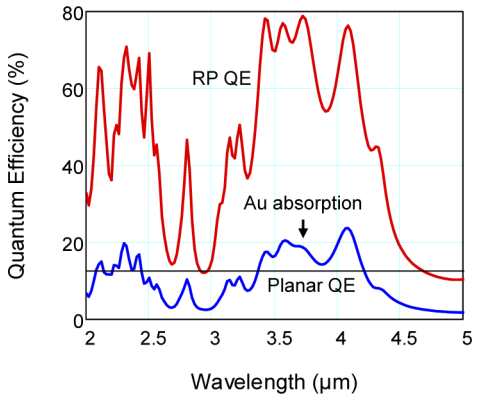

Fig. 4. The modeled QE with the optimized detector parameters for constant $\alpha = 2000$ cm^{-1}.

To use the same RP geometry for light emission, we first characterize its properties as a passive resonator, in which the absorber is replaced by a dielectric of the same n = 3.735 but with extinction coefficient k = 0. In this case, the optical loss is either from the ohmic attenuation in the gold layer or from the outgoing radiation at the substrate/air interface. Explicit EM modeling confirms that the sum of these two losses is exactly equal to the incident power P_{in} as required by energy conservation. Therefore, the quality factor Q of the resonator can be obtained from

$$Q = 2\pi f \frac{U_s}{R} = \frac{\pi c n^2 \varepsilon_0}{\lambda} \frac{\int_V |E(r)|^2 d^3 r}{P_{in}} \quad , \tag{4}$$

where $f = c/\lambda$ is the optical frequency, $U_s = \frac{1}{2}\varepsilon_r \varepsilon_0 |E(r)|^2$ is the energy density stored in the dielectric resonator, and $R = P_{in}$ is the total energy dissipation rate, and V is the dielectric volume. Explicit modeling shows the energy stored in the gold cover is 4 orders of magnitude lower than that in the dielectric layer because of the small field penetration, and therefore it can be neglected in the total stored energy in Eq. (4). Since the photon number in the resonator r relative to a planar dielectric is also directly proportional to U_s, r and Q are generally related, though not strictly proportional, as seen in Fig. 5. The value of r has a local maximum of 29.8 while that of Q is 57.1 at 4.08 μm due to the large plasmonic enhanced E field in the dielectric volume.

Optics EXPRESS

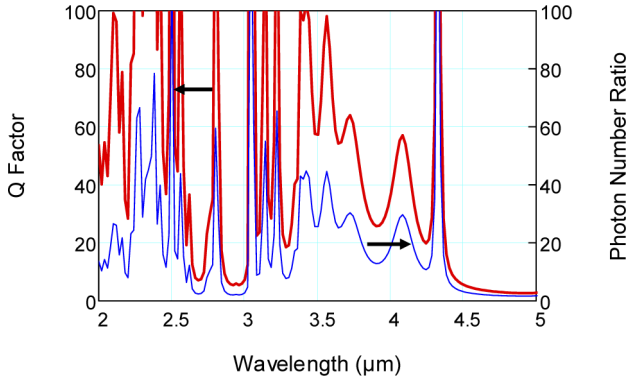

Fig. 5. The Q factor of the resonator and the number of photons in the dielectric layer of the resonator relative to a semi-infinite block of the same medium.

From the stored E field, the effective mode volume V_{eff} can also be computed from [26]

$$V_{eff} = \frac{\int_V \varepsilon_r(r)|E(r)|^2 d^3r}{max(\varepsilon_r(r)|E(r)|^2)} = \frac{\int_V |E(r)|^2 d^3r}{max(|E(r)|^2)} \left(\frac{n}{\lambda}\right)^3 \left(\frac{\lambda}{n}\right)^3 = v\left(\frac{\lambda}{n}\right)^3 , \quad (5)$$

where v is the mode volume in the unit of $(\lambda/n)^3$. The value of V_{eff} is shown in Fig. 6(a). The smallest $v = 3.44 \times 10^{-3}$ occurs at 4.08 μm, signaling the presence of the very intense E field at this λ. This very small v is a signature of the creation of LSPs. Due to the 4-fold rotational symmetry of the present structure, Q and V_{eff} are independent of the incident polarization angle θ in the x-y plane. In order to facilitate the following discussion, we will first select a specific θ of 45° and return to other angles later. With equal incident E_{0x} and E_{0y} components, the maximum E field is located along the diagonal cross-section of the ring. A plot of the E field in this cross-section in Fig. 7(a) shows that $|E|^2$ near the corner of the gold ring can be 2465 times larger than the incident $|E_0|^2$. With a large Q and a small V_{eff}, the Purcell factor F_p given by

$$F_p = \frac{3}{4\pi^2}\left(\frac{\lambda}{n}\right)^3 \frac{Q}{V_{eff}} , \quad (6)$$

can be large at 1261 in Fig. 6(b). Since the spontaneous emission rate of an emitter is directly proportional to F_p of the cavity mode, and if the dielectric is replaced by an LED material, the emission rate near the ring corner will increase by 1261 times. Therefore, the light emission of the RP emitter will be highly concentrated in the corners at $\lambda = 4.08$ μm for this polarization. Note that the values $|E|^2$ are computed at the discretization nodes in the FEM analysis and their maximum value, the deduced mode volume, and F_p can be somewhat different using different computation mesh. Nevertheless, the average recombination rate from the entire volume, which is a function of the average photon energy density in the resonator, is independent of the computation mesh, and it is $r = 29.8$ times larger than that of a planar medium.

Figure 7(b) shows the direction of the optical E fields near the opposite corners of the ring. They are 180° out of phase: one is pointing primarily up while the other is pointing primarily down. From cavity QED [11,26], the optical emission characteristics of an optical emitter is strongly modified by the optical cavity. In particular, the Purcell enhanced spontaneous optical emission is driven by the quantum fluctuation (i.e. random occurrence) of the cavity mode rather than the free-space vacuum modes. Its transition matrix element is the largest when the spatially distributed dipole moment is aligned and in phase with the E field of the cavity mode. The optical emission of the resonator is therefore primarily driven by the coherent dipole oscillations in the

Optics EXPRESS

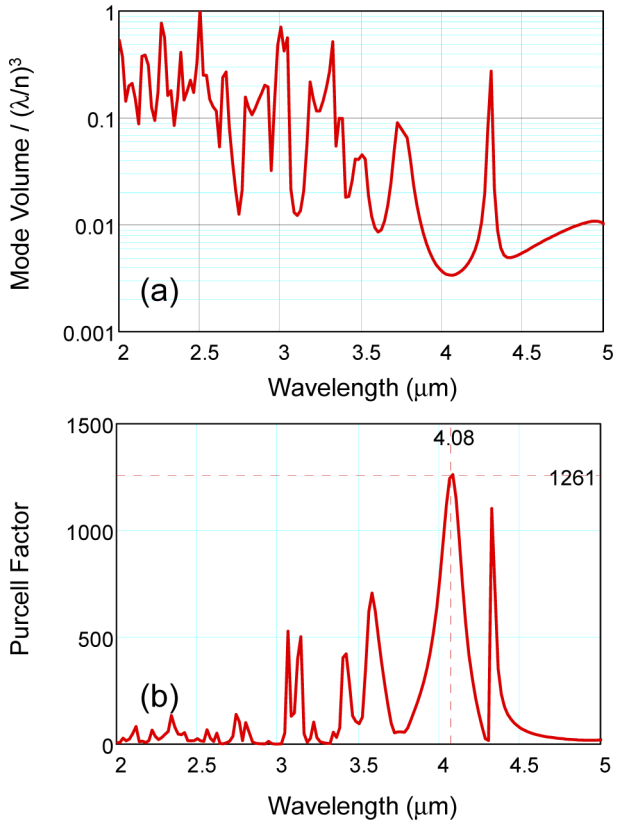

Fig. 6. (a) The effective mode volume in the unit of $(\lambda/n)^3$, (b) The Purcell enhancement factor for spontaneous emission.

opposite corners of the ring for this polarized emission. This dipole orientation is similar to that in the interband cascade light-emitting device studied in Ref. 24, in which the cavity E field is in opposite directions in the alternate light emitting layers.

To simulate this radiation, a pair of AC current feedlines are placed in the diagonal positions indicated in Fig. 8. Each driving current is 10 mA and they are in opposite phase. The resulting power radiated into free space P_{out} is shown in Fig. 9(a) for the electrical driving power P_{in}. The oscillatory P_{in} indicates that the resonator behaves as a radiating antenna, exhibiting varying feed impedance at different λ. Besides P_{out}, Fig. 9(a) also shows the computed absorbed power P_{abs} in the gold layer, which is dissipated as heat. The sum of P_{out} and P_{abs} turns out to be equal to the driving power P_{in} within a modeling error of 0.1%.

The radiation efficiency or, more appropriately, the light extraction efficiency η_{LEE} of the RP emitter, given by P_{out}/P_{in}, is shown in Fig. 9(b). The value of η_{LEE} can be larger than 80% compared to the ~2% of a planar LED. While the maximum power is obtained at 4.08 μm, the maximum η_{LEE} occurs at 3.88 μm because of the less gold absorption shown in Fig. 9(a) at this wavelength. This result shows that if the LED emits light around 4 μm with this polarization, it will emit into this plasmonic cavity mode at a Purcell-enhanced spontaneous emission rate and creates intensity maxima at the diagonal corners. The resonator does not only increase the radiative recombination rate by 30 times but also facilitates the optical energy to radiate out into free space at a high extraction efficiency of 80%, resulting in a much larger external quantum efficiency η_{ext}. Note the spectral similarity between the absorption quantum efficiency η in Fig. 4

Optics EXPRESS

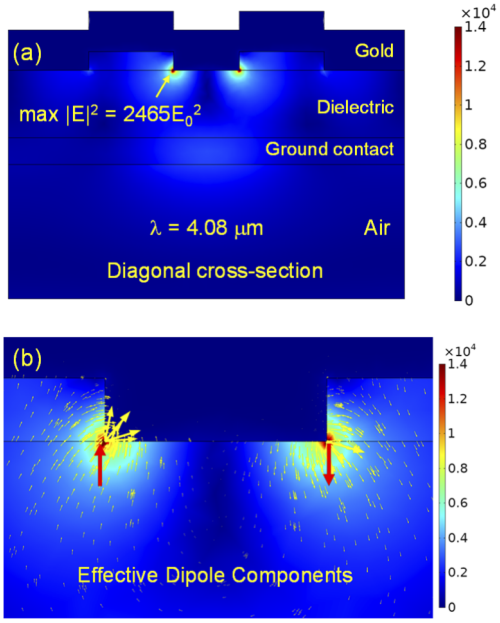

Fig. 7. (a) The diagonal cross-section of a RP emitter showing the optical |E| when the incident $E_0 = 532.8$ V/m of equal x and y amplitudes. (b) The E directions near the diagonal corners.

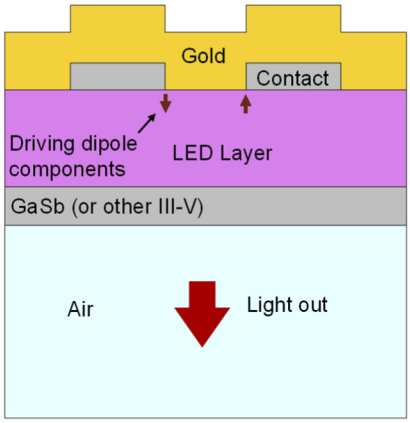

Fig. 8. The locations of the driving dipoles in a RP emitter.

and the extraction efficiency η_{LEE} in Fig. 9(b) as dictated by the antenna reciprocity theorem. They are not exactly the same only because of the approximate nature of the simulated dipole positions and orientations.

Figures 10 and 11 show the downward optical power density in different detector cross-sections. Cut plane 2 shows a strong downward power (in red) radiated from the center of the ring, and a portion of it transmits into the air. In cut plane 1, which is 0.2 μm below the gold cover, there is power propagating upward around the ring (in dark blue) as well as downward at the center of the ring (in red). This power pattern shows the optical beam is circulating inside the resonator before it transmits out of the volume. In cut plane 3, which is 2 μm into the air below the substrate, the emitted power becomes spatially uniform. This example shows that the RP geometry used

Optics EXPRESS

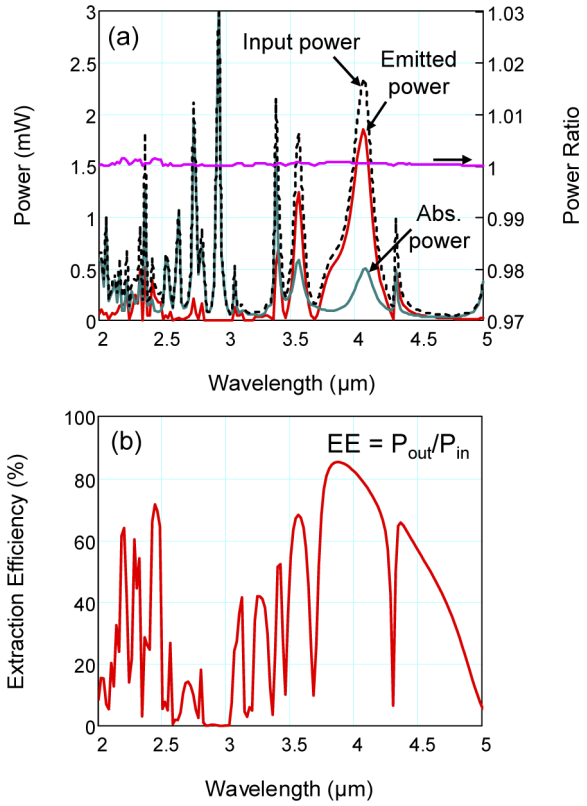

Fig. 9. (a) The computed electrical driving input power P_{in} (dashed curve), the emitted optical power P_{out} in the air (red curve), the absorbed power P_{abs} in the gold layer, and the power ratio $(P_{out} + P_{abs})/P_{in}$. (b) The extraction efficiency = P_{out}/P_{in} of the RP emitter.

for detection is also efficient in surface emission, and the RP emitter is performing the inverse function of an RP detector.

The above analysis is for the emission polarized at 45°. It is however equally applicable to any other polarization angles. When the emission E_0 is at an arbitrary angle, E_0 can be decomposed into two orthogonal E_{45} and E_{-45} components. Due to the symmetry of the ring, E_{-45} will produce proportionally the same mirror-reflected electric field distribution and thus has the same light extraction efficiency as E_{45} calculated in Fig. 9(b). Since both components have the same LEE, it follows that LEE of the combined E_0 will also be the same. Therefore, the optical intensity from the RP emitter is independent of the polarization angle and is isotropic. Note that although different polarizations share the same LEE, the E field distribution of each polarization, which is the superposition of the two components' distributions, is different for each angle. Therefore, the overall radiation from the RP emitter is emitted from around the ring rather than only from the corners. From Fig. 7, the plasmonic field is primarily localized in the upper half of the light emitting layer, one can further optimize the active layer thickness t_d for the same total thickness $t_d + t_g$ to yield a better emission to reabsorption ratio in the active layer.

Since IQE of different materials can vary widely, depending on the band structure and emission wavelength, it is useful to evaluate EQE of the RP structure at different IQE values observed in a planar structure. If a planar emitter has a LEE of 2% and an IE of 50%, which also includes power loss to the contact and internal series resistence, EQE will reduce by a factor of 100 from its IQE. Even when IQE is ideal at 100%, EQE can only be 1%, which is the reason for the

Optics EXPRESS

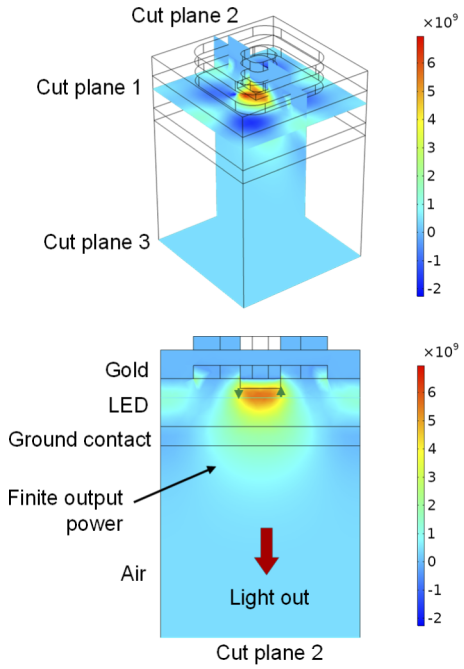

Fig. 10. The 3D view of the RP emitter and the power profiles in the unit of Wm^{-2} in different cut planes at $\lambda = 4.08$ μm.

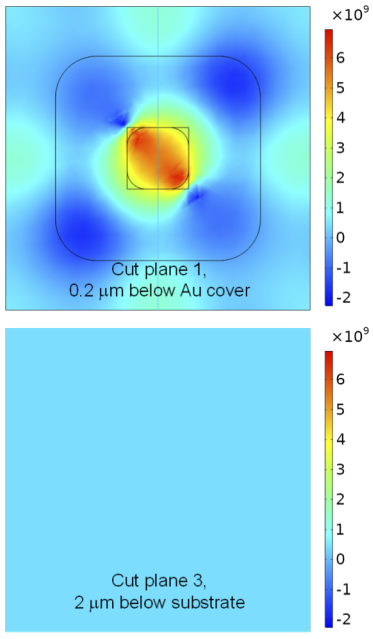

Fig. 11. The power profiles in the unit of Wm^{-2} in two different horizontal cut planes at $\lambda = 4.08$ μm.

Optics EXPRESS

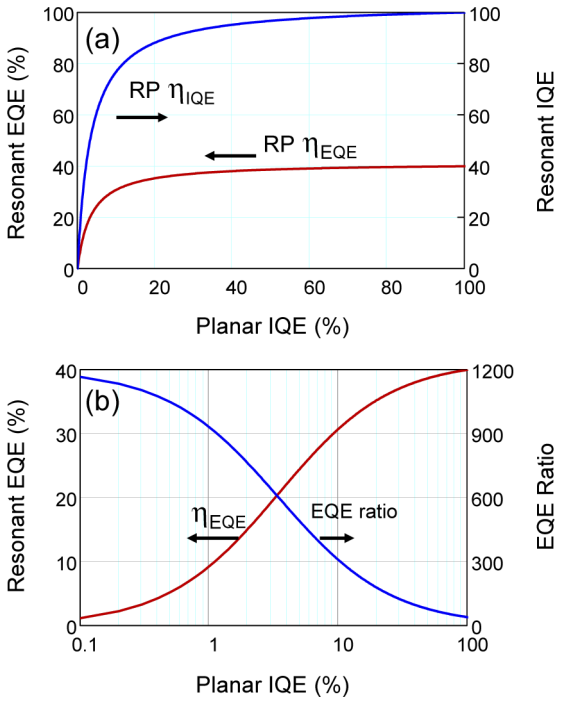

Fig. 12. The IQE and EQE of a RP emitter as a function of the planar IQE. (b) The RP emitter EQE and its ratio relative to a planar LED at different planar IQE.

small EQE in many LEDs, especially in the infrared wavelengths [24]. A common approach in increasing LEE is to encapsulate the LEDs within a transparent plastic dome of a lesser refractive index. However, this approach is less applicable to large area LED arrays designed for normal illumination.

From Fig. 5, the volumetric averaged photon density in the resonator is 30 times larger than that in a planar medium at 4.08 μm. Consequently, the square of the transition matrix element and thus the radiative recombination rate are 30 times larger. The IQE in a resonator, η_{res}, is then given by

$$\eta_{res} = \frac{30 \times \eta_{pl}}{30 \times \eta_{pl} + (1 - \eta_{pl})} \quad , \tag{7}$$

where η_{pl} is the original IQE of the planar emitter. In Fig. 12(a), the RP IQE is plotted against the planar IQE. The RP IQE rises rapidly and reaches $\eta_{res} = 88.2\%$ at $\eta_{pl} = 20\%$. With a LEE of 80% for the RP emitter and the same IE of 50%, the RP EQE will be 35.3% while the corresponding planar EQE is only 0.2%. Since the RP improvement is larger at smaller η_{pl}, we plot the RP EQE and its ratio relative to the planar EQE in logarithmic scale in Fig. 12(b). At $\eta_{pl} = 0.1\%$, the RP EQE = 1.2%, which is 1166 times larger than the planar EQE. At another extreme where $\eta_{pl} = 100\%$, the RP EQE = 40%, and it is 40 times larger. Therefore, the RP structure can substantially improve the planar EQE in the entire η_{pl} range.

4. Resonator-pixel thermal emitters

Other than enhancing LED performance, metal nanostructures have also been used to improve the thermal emission properties of a material for applications such as thermophotovoltaic (TPV) power generation [25,27] and infrared gas sensing [28,29]. Similarly, resonator-pixel structures are also beneficial in passive thermal emission. Different from the usual approaches in which

Optics EXPRESS

metal nanostructures such as photonic crystals or metastructures are placed on top of the emitter surface, the ring structure of the RP thermal emitter is placed at the back of the surface, with which the micro-scaled structure can be better protected from the air exposure. In a RP thermal emitter, the active light emitting region and the ground contact region are replaced by a dielectric material such as SiC that can be heated to 1500°C or higher for TPV applications. For the same reason, the ring cover is also replaced by a metal with high melting points (MPs) such as tantalum. At 1500°C, the blackbody radiation is peaked around 2 μm. Therefore, the RP emitter is designed with a peak emissivity ε at 1.8 μm. By Kirchhoff's law, the emitter should show the same peak absorptivity at the same 1.8 μm [28]. Figure 13 shows the optimized structure for the 1.8 μm emission, which is based on Ta and SiC materials with their refractive index shown in Fig. 14.

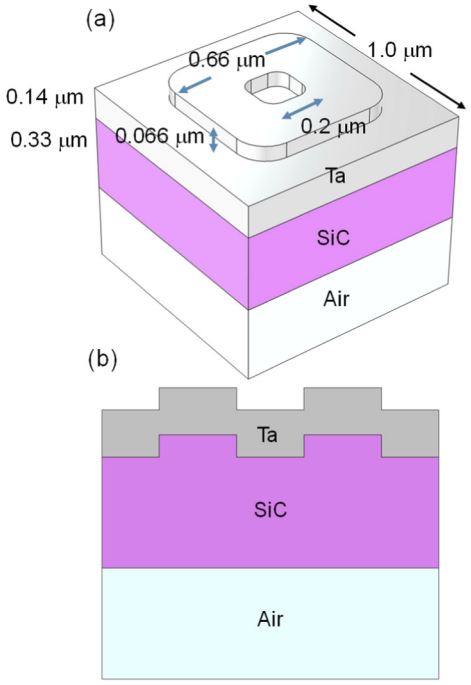

Fig. 13. The 3-D view and the cross-sectional view of a passive RP radiator for 1.8 μm emission.

Figure 15 shows that at $\lambda = 1.8$ μm, a large LSP field is created at the corners of the rings, similar to the active LED case. Figure 16(a) shows the modeled emissivity spectrum of the RP emitter, which is obtained by equating it to the external QE [28]. When the emitter is heated to 1500°C, the structure emits the blackbody radiation modified by the emissivity spectrum. Figure 16(b) shows the emission spectrum of the emitter relative to a blackbody. The emitter is able to emit 65.1% of blackbody power with $\lambda < 1.9$ μm and only 15.0% with $\lambda > 1.9$ μm. When the emitter is used with a GaSb photodiode whose cutoff is at 1.9 μm for TPV application, the cooling requirement will be reduced by 85% because of the reduced radiated power at the longer wavelengths. This level of performance is very similar to that of the 3D photonic crystals [25].

In the above example, we used tantalum as the cover material. With its a high MP of 2980°C, this material is well suited for TPV applications. We have modeled other metals with MP higher than 1500°C except that of gold, and their performance is listed in Table 1 below. A good emitter should have a high emitting power shorter than 1.9 μm and a low emitting power longer than 1.9 μm. Therefore, the figure of merit is the power selectivity, which is defined as the ratio of the short wavelength power to the long wavelength power. From Table 1, one can observe that gold

Optics EXPRESS

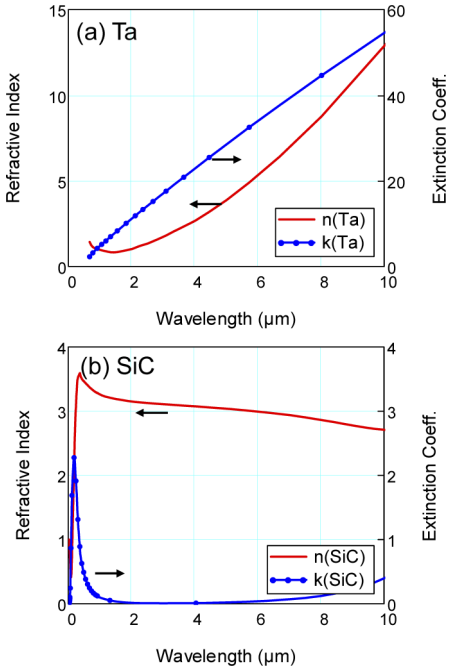

Fig. 14. The refractive index of (a) Ta and (b) SiC adopted in the EM modeling.

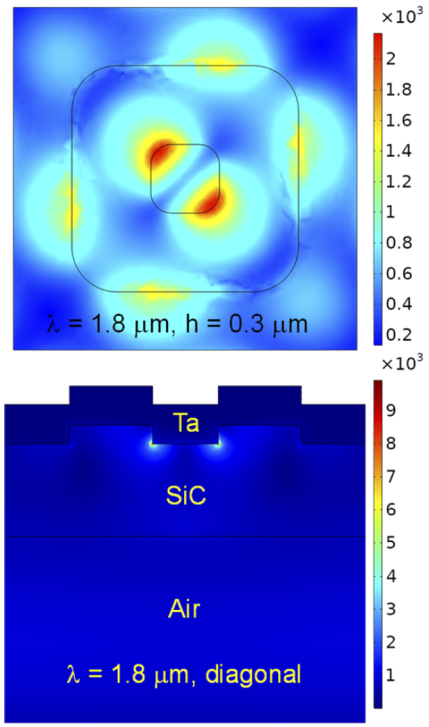

Fig. 15. The top view of the E distribution at a height of 0.3 μm above the SiC/air interface and the cross-diagonal view of the E distribution when the incident E_0 = 532.8 V/m of equal x and y amplitudes.

Optics EXPRESS

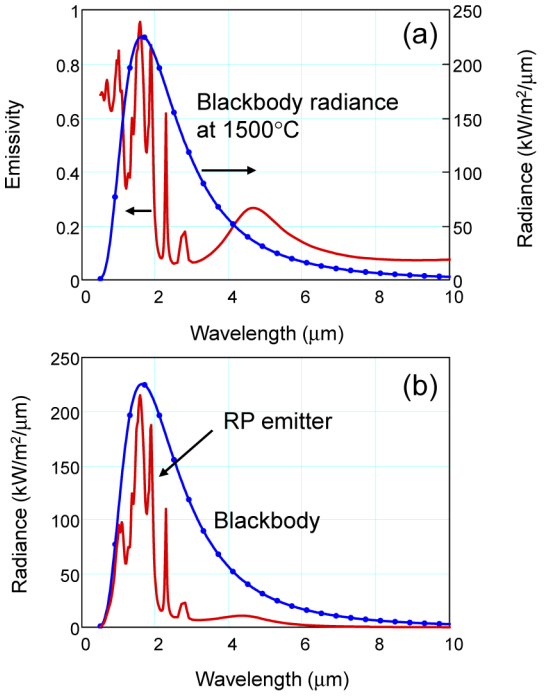

Fig. 16. (a) The emissivity spectrum of the passive RP thermal emitter and the 1500°C blackbody radiation. (b) The emission spectrum of the RP emitter when heated to 1500°C compared to the blackbody spectrum.

actually has the highest power selectivity of 5.84 although its low MP makes it unsuitable for this application. The next choice will be tantalum with its value of 4.34. Since Ta is also a relatively low cost material, it may offer a good choice.

Table 1. Power Selectivity with Different Metal Covers

	Gold	Tungsten	Rhodium	Tantalum	Niobium	Chromium	Platinum
Melting point (°C)	1063	3400	3186	2980	2470	1860	1770
P_{emit}/P_{BB} (< 1.9 μm)	0.629	0.706	0.708	0.651	0.677	0.745	0.729
P_{emit}/P_{BB} (> 1.9 μm)	0.108	0.206	0.193	0.150	0.204	0.325	0.291
Power selectivity	5.84	3.43	3.68	4.34	3.32	2.29	2.51

5. Conclusion

In this work, we perform 3-dimensional electromagnetic modeling to design and optimize a light emitting device with a micro-scaled photonic structure. With this photonic structure, there is coherent cycling of energy between the light emitting medium and the localized surface plasmon. In the weak coupling regime, the light emission rate into the plasmonic mode is increased by the Purcell factor of 30 times. Cavity QED stipulates the preferential emission into the LSP mode occurring at highly localized regions because of the very small mode volume. Since this LSP mode is designed to be a radiating mode of the resonator, the optical energy can be efficiently radiated into free space. Explicit EM modeling by placing oscillating dipoles in the localized regions predicts a light extraction efficiency that is 40 times larger than the planar LEDs with the rest of the optical energy being dissipated in the metal cover. The combined external

Optics EXPRESS

quantum efficiency of the resonator-pixel emitter can thus be much larger than that of a planar emitter. In addition to the active emitter, we also designed a passive emitter, which suppresses the thermal emission by 85% below a cutoff wavelength with Ta cover, thus lessening the cooling requirement in thermophotovoltaic applications. Even though we only designed emitters in the infrared region, emitters at other emission wavelengths can be similarly designed by scaling the emitter geometrical dimensions proportionally and thus the device concept can be applied to many technological areas. However, we should emphasize that since the present device concept involves multiple branches of physics and certain operation details have been ignored such as the carrier injection and transport, this device concept will need further refinement and experimental confirmation before its benefits can be fully evaluated.

Funding. Banpil Photonics internal research.

Disclosures. The authors declare no conflicts of interest.

Data availability. Data underlying the results presented in this paper are not publicly available at this time but may be obtained from the authors upon reasonable request.

References

1. E. Matioli and C. Weisbuch, "Active Region Part A. Internal Quantum Efficiency in LEDs," Topics in Applied Physics **126**, 121–152 (2013).
2. H. Benisty, H. De Neve, and C. Weisbuch, "Impact of Planar Microcavity Effects on Light Extraction—Part I: Basic Concepts and Analytical Trends," IEEE J. Quant. Elect. **34**(9), 1612–1631 (1998).
3. J. Zhang, L. Zhang, and Wei Xu, "Surface plasmon polaritons: physics and applications," J. Phys. D: Appl. Phys. **45**(11), 113001 (2012).
4. Y. Zhong, S. D. Malagari, T. Hamilton, and D. Wasserman, "Review of mid-infrared plasmonic materials," J. Nanophotonics **9**(1), 093791 (2015).
5. X. Gu, T. Qiu, W. Zhang, and P. K. Chu, "Light-emitting diodes enhanced by localized surface plasmon resonance," Nanoscale Res Lett **6**(1), 199 (2011).
6. K. Okamoto, I. Niki, A. Shvartser, Y. Narukawa, T. Mukai, and A. Scherer, "Surface-plasmon-enhanced light emitters based on InGaN quantum wells," Nature Mater **3**(9), 601–605 (2004).
7. A. Fujiki, T. Uemura, N. Zettsu, M. Akai-Kasaya, A. Saito, and Y. Kuwahara, "Enhanced fluorescence by surface plasmon coupling of Au nanoparticles in an organic electroluminescence diode," Appl. Phys. Lett. **96**(4), 043307 (2010).
8. K. Huang, N. Gao, C. Wang, X. Chen, J. Li, S. Li, X. Yang, and J. Kang, "Top- and bottom-emission-enhanced electroluminescence of deep-UV light-emitting diodes induced by localised surface plasmons," Sci Rep. **4**, 4380 (2014).
9. N. Kim, S. Hong, J. Kang, N. Myoung, S.-Y. Yim, S. Jung, K. Lee, C. W. Tue, and S.-J. Park, "Localized surface plasmon-enhanced green quantum dot light-emitting diodes using gold nanoparticles," RSC Adv. **5**(25), 19624–19629 (2015).
10. R. M. Bakker, H.-K. Yuan, Z. Liu, V. P. Drachev, A. V. Kildishev, and V. M. Shalaev, "Enhanced localized fluorescence in plasmonic nanoantennae," Appl. Phys. Lett. **92**(4), 043101 (2008).
11. D. A. Steck, *Quantum and Atom Optics*, available online at http://steck.us/teaching (revision 0.11.5, 27 November (2016), ch. 10.
12. J.B. Khurgin, "How to deal with the loss in plasmonics and metamaterials," Nature Nanotech **10**(1), 2–6 (2015).
13. J. B. Pendry, L. Martın-Moreno, and F. J. Garcia-Vidal, "Mimicking Surface Plasmons with Structured Surfaces," Science **305**(5685), 847–848 (2004).
14. K. K. Choi, M. D. Jhabvala, J. Sun, C. A. Jhabvala, A. Waczynski, and K. Olver, "Resonator-quantum well infrared photodetectors," Appl. Phys. Lett. **103**(20), 201113 (2013).
15. K. K. Choi, M. D. Jhabvala, D. P. Forrai, A. Waczynski, J. Sun, and R. Jones, "Electromagnetic modeling and design of quantum well infrared photodetectors," IEEE J. Select. Topics Quantum Electron. **19**(5), 1–10 (2013).
16. K. K. Choi, "Metastructures for VLWIR SLS detectors," Proc. SPIE **11407**, 114070K1 (2020).
17. K. K. Choi, A. K. Dutta, and N. K. Dhar, "High Performance Infrared Photodetectors and Energy Harvesting Devices Based on Micro-Scaled Photonics Structures," IEEE J. Quantum Electron. **57**(4), 1–10 (2021).
18. A. K. Dutta, A. Suzuki, K. Kurihara, F. Miyasaka, H. Hotta, K. Sugita, and K. , "High-Brightness, AlGaInP-Based, Visible Light-Emitting Diode for Efficient Coupling with POF," IEEE Photon. Technol. Lett. **7**, 1134–1136 (1995).
19. A. K. Dutta, K. Ueda, K. Hara, and K. Kobayashi, "High brightness and reliable AlGaInP-based light emitting diode for POF data links," IEEE Photon. Technol. Lett. **9**(12), 1567–1569 (1997).
20. A. K. Dutta, "Prospects of highly efficient AlGaInP based surface emitting type ring-LED for 50 and 156 Mb/s POF data link systems," J. Lightwave Technol. **16**(1), 106–113 (1998).
21. A. K. Dutta, K. Hara, K. Kobayashi, and N. Nagashima, "Impedance, modulation response and equivalent-circuit of 650nm surface emitting type light-emitting diode for POF data-links," Solid-State Electron. **42**, 1781–1791 (1998).

Optics EXPRESS

22. A. K. Dutta, Japan Patent: JP2783210, Light Emitting Diode, Assignee NEC Corp., Granted August 6, 1998.
23. F. A. Al-Saymari, A. P. Craig, Qi Lu, A. R. J. Marshall, P. J. Carrington, and A. Krier, "Mid-infrared resonant cavity light emitting diodes operating at 4.5 µm," Opt. Express **28**(16), 23338–23353 (2020).
24. C. S. Kim, M. Kim, W. W. Bewley, C. D. Merritt, C. L. Canedy, M. V. Warren, I. Vurgaftman, and J. R. Meyer, "Mid-Infrared Interband Cascade Light-Emitting Devices with Improved Radiance," Proc. SPIE **10540**, 105400 (2018).
25. S. Y. Lin, J. G. Fleming, E. Chow, J. Bur, K. K. Choi, and A. Goldberg, "Enhancement and suppression of thermal emission by a three-dimensional photonic crystal," Phys. Rev. B **62**(4), R2243–R2246 (2000).
26. J. Vučković, "Quantum optics and cavity QED with quantum dots in photonic crystals," in *Quantum Optics and Nanophotonics*, Oxford University Press, Oxford, (2017).
27. N. A. Pfiester and T. E. Vandervelde, "Selective emitters for thermophotovoltaic applications," Phys. Status Solidi A **214**(1), 1600410 (2017).
28. D. Costantini, A. Lefebvre, A.-L. Coutrot, I. Moldovan-Doyen, J.-P. Hugonin, S. Boutami, F. Marquier, H. Benisty, and J.-J. Greffet, "Plasmonic Metasurface for Directional and Frequency-Selective Thermal Emission," Phys. Rev. Appl. **4**(1), 014023 (2015).
29. A. Lochbaum, Y. Fedoryshyn, A. Dorodnyy, U. Koch, C. Hafner, and J. Leuthold, "On-Chip Narrowband Thermal Emitter for Mid-IR Optical Gas Sensing," ACS Photonics **4**(6), 1371–1380 (2017).